Single slit diffraction: from optics to elasticity

A. Berezovski[a,*], J.Engelbrecht[a]

[a] *Institute of Cybernetics at Tallinn University of Technology, Akadeemia tee 21, Tallinn 12618, Estonia*

Abstract

The comparison of numerical simulations of the classical problem of the single slit diffraction in optical, acoustic, and elastic cases are presented in the paper in the plane strain setting. It is shown that wave fields downstream the slit are similar in optical and acoustic cases, as expected. Corresponding wave fields in the single slit diffraction using elastic materials become essentially different from optical and acoustic cases. This is an effect of elastic waves propagating inside the plate forming the slit.

Keywords: elastic wave, diffraction, single slit, numerical simulation

2010 MSC: 74B05, 74J20, 65N08

1. Introduction

Diffraction is a well studied phenomenon, especially in classical optics since the celebrated Tomas Young double slit diffraction experiment (Young, 1804) demonstrated the wave-like behaviour of light. In elasticity, much attention was paid to scattering problems due to their practical application (Mow & Pao, 1971; Hellier & Hellier, 2001). Since diffraction and scattering are complementary phenomena, the same mathematical technique is used in their description, especially in acoustics, because of identity of the wave propagation equation in acoustics and classical optics (De Hoop, 2008). The conversion of longitudinal and shear waves at boundaries in scattering and diffraction problems in

*Corresponding author

Email address: Arkadi.Berezovski@cs.ioc.ee (A. Berezovski)

elasticity makes the corresponding solution much more complicated.

The emerging field of metamaterials (composites with unusual macroscopic properties due to local resonances) provides an unprecedented way for controlling wave propagation in a desired way by tailoring the microstructure (Deymier, 2013). Simultaneously, it demands a more precise prediction of the wave field. The problem of wave propagation through heterogeneous materials has been considered since the mid-nineteenth century (Rayleigh, 1887), and since then the progress in considering ever more complicated scattering structures has been continuous (Auld, 1973; Graff, 1975; Achenbach, 1984). Various approaches to predicting the wave propagation through different scattering structures have recently been reviewed by Martin (2006) and Harris (2010).

Analytical difficulties often lead to the restriction of the analysis by limiting cases of very short wavelengths (ultrasound) and of very long wavelengths (quasi-statics). It is remarkable that the elastic analogue of the Talbot effect known in classical optics for a long time (Talbot, 1836) has been demonstrated only recently (Berezovski et al., 2014). The reason is in the comparability of wavelengths with the slit size of the grating in the elastic case.

The prediction of the wave field is the key element in the wave control. The growth of computer power and the progress in numerical methods provide a direct numerical solution of diffraction problems. The major advantage of numerical simulation is its generality and the capability of predicting wave fields for any composite with arbitrarily distributed scatterers.

Before the application of numerical simulations to complicated situations, it is instructive to start with one of the basic problems - the single slit diffraction. This problem is studied in detail in classical optics both theoretically and experimentally (Benenson et al., 2002). Classical optics is characterized by the extremely short wavelength in comparison to the slit size, while in acoustics the wavelength and the slit size may have the same order of magnitude. The absence of shear waves is common for both optics and acoustics. It should be noted, however, that traditionally the plate forming a slit is opaque (not transparent) in optics and perfectly rigid in acoustics. The completely elastic formulation of the single slit diffraction suggests the elastic behavior both for the matrix and for the plate forming the slit.

In the paper, we try to emphasize the similarity and the difference between the single slit diffraction in optics, in acoustics, and in elasticity demonstrating numerically calculated wave fields. The major difference of the elastic case from the classical single slit diffraction in optics and acoustics is due to the propagation of wave through the matrix as well as through the plate forming the slit, which is not present in classical optics and in acoustics case. Additionally, both longitudinal and shear waves are accounted for in the elastic case, while in acoustics only longitudinal waves are taken into account. The variation of the thickness of the plate forming the slit is also analysed. This will permit us later to understand better the influence of geometrical shapes of gratings and possible nonlinearities of materials.

The paper is organized as follows. In Section 2 we introduce the governing equations for the plain strain elasticity and present their non-dimensional form in Section 3. In Section 4 numerical results for various cases are presented based on applying the modified wave-propagation algorithm (Berezovski & Maugin, 2001; Berezovski et al., 2008). The corresponding governing equations are specified with suitable scaling and assumptions. Section 5 includes conclusions and some ideas for further studies.

2. Plane strain elasticity

Numerical simulation of elastic wave propagation is based on the solution of equations of elasticity. Although the governing equations are well-known, we represent here the basic forms in order to explain later the possible simplifications. Neglecting both geometrical and physical nonlinearities, we can write the bulk equations of homogeneous linear isotropic elasticity in the absence of body force as follows (Barber, 2009):

$$\rho_0 \frac{\partial v_i}{\partial t} = \frac{\partial \sigma_{ij}}{\partial x_j}, \tag{1}$$

$$\frac{\partial \sigma_{ij}}{\partial t} = \lambda \frac{\partial v_k}{\partial x_k} \delta_{ij} + \mu \left(\frac{\partial v_i}{\partial x_j} + \frac{\partial v_j}{\partial x_i} \right), \tag{2}$$

where t is time, x_j are spatial coordinates, v_i are components of the velocity vector, σ_{ij} is the Cauchy stress tensor, ρ_0 is the density, λ and μ are the Lamé coefficients.

Consider a sample that is relatively thick along x_3, and where all applied forces are uniform in the x_3 direction. Since all derivatives with respect to x_3 vanish, all fields can be viewed as functions of x_1 and x_2 only. This situation is called plane strain. The corresponding displacement component (e.g., the component u_3 in the direction of x_3) vanishes and the others (u_1, u_2) are independent of that coordinate x_3; that is,

$$u_3 = 0, \quad u_i = u_i(x_1, x_2), \quad i = 1, 2. \tag{3}$$

It follows that the strain tensor components, ε_{ij} are

$$\varepsilon_{i3} = 0, \quad \varepsilon_{ij} = \frac{1}{2}(u_{i,j} + u_{j,i}), \quad i, j = 1, 2. \tag{4}$$

The stress components follow then

$$\sigma_{3i} = 0, \quad \sigma_{33} = \frac{E}{1 - 2\nu} \left(\frac{\nu}{1 + \nu} \varepsilon_{ii} \right), \quad i = 1, 2. \tag{5}$$

$$\sigma_{ij} = \frac{E}{1 + \nu} \left(\varepsilon_{ij} + \frac{\nu}{1 - 2\nu} \varepsilon_{kk} \delta_{ij} \right), \quad i, j, k = 1, 2, \tag{6}$$

where E is the Young's modulus, ν is the Poisson's ratio, δ_{ij} is the unit tensor.

Inversion of Eq. (6) yields an expression for the strains in terms of stresses:

$$\varepsilon_{ij} = \frac{1 + \nu}{E} \left(\sigma_{ij} - \nu \sigma_{kk} \delta_{ij} \right), \quad i, j, k = 1, 2. \tag{7}$$

System of Eqs. (1)-(2), specialized to plane strain conditions by Eqs. (3)-(7), has the form

$$\rho \frac{\partial v_1}{\partial t} = \frac{\partial \sigma_{11}}{\partial x} + \frac{\partial \sigma_{12}}{\partial y}, \tag{8}$$

$$\rho \frac{\partial v_2}{\partial t} = \frac{\partial \sigma_{21}}{\partial x} + \frac{\partial \sigma_{22}}{\partial y}. \tag{9}$$

Accordingly, compatibility conditions are represented as

$$\frac{\partial \varepsilon_{11}}{\partial t} = \frac{\partial v_1}{\partial x}, \tag{10}$$

$$\frac{\partial \varepsilon_{12}}{\partial t} = \frac{1}{2}\left(\frac{\partial v_1}{\partial y} + \frac{\partial v_2}{\partial x}\right), \tag{11}$$

$$\frac{\partial \varepsilon_{22}}{\partial t} = \frac{\partial v_2}{\partial y}. \tag{12}$$

Stress-strain relations (the Hooke's law) close the system of governing equations

$$\sigma_{11} = (\lambda + 2\mu)\varepsilon_{11} + \lambda\varepsilon_{22}, \tag{13}$$

$$\sigma_{12} = \sigma_{21} = 2\mu\varepsilon_{12}, \tag{14}$$

$$\sigma_{22} = (\lambda + 2\mu)\varepsilon_{22} + \lambda\varepsilon_{11}. \tag{15}$$

Time derivatives of stress-strain relations accounting the compatibility conditions determine

$$\frac{\partial \sigma_{11}}{\partial t} = (\lambda + 2\mu)\frac{\partial v_1}{\partial x} + \lambda\frac{\partial v_2}{\partial y}, \tag{16}$$

$$\frac{\partial \sigma_{22}}{\partial t} = \lambda\frac{\partial v_1}{\partial x} + (\lambda + 2\mu)\frac{\partial v_2}{\partial y}, \tag{17}$$

$$\frac{\partial \sigma_{12}}{\partial t} = \frac{\partial \sigma_{21}}{\partial t} = \mu\left(\frac{\partial v_1}{\partial y} + \frac{\partial v_2}{\partial x}\right). \tag{18}$$

These equations together with the balance of linear momentum (8)–(9) form the system of equations, which is convenient for a numerical solution.

3. Nondimensional equations

In the single-slit problem we have three independent space scales:

- the slit size a,
- the width of the plate (the slit thickness) w,
- the wavelength L.

The time scale is determined by means of the longitudinal wave speed c_p and the reference wavelength L as follows:

$$t_0 = \frac{L}{c_p}. \tag{19}$$

Introducing dimensionless variables

$$X = \frac{x}{a}, \quad Y = \frac{y}{w}, \quad T = \frac{t}{t_0} = \frac{tc_p}{L}, \tag{20}$$

and dimensionless unknowns

$$V_i = \frac{v_i}{c_p}, \quad \Sigma_{ij} = \frac{\sigma_{ij}}{\sigma_0}, \tag{21}$$

we can re-write the governing equations in the form

$$\frac{\rho c_p^2}{L}\frac{\partial V_1}{\partial T} = \frac{\sigma_0}{a}\frac{\partial \Sigma_{11}}{\partial X} + \frac{\sigma_0}{w}\frac{\partial \Sigma_{12}}{\partial Y}, \tag{22}$$

$$\frac{\rho c_p^2}{L}\frac{\partial V_2}{\partial T} = \frac{\sigma_0}{a}\frac{\partial \Sigma_{21}}{\partial X} + \frac{\sigma_0}{w}\frac{\partial \Sigma_{22}}{\partial Y}. \tag{23}$$

$$\frac{\sigma_0 c_p}{L}\frac{\partial \Sigma_{11}}{\partial T} = \frac{(\lambda+2\mu)c_p}{a}\frac{\partial V_1}{\partial X} + \frac{\lambda c_p}{w}\frac{\partial V_2}{\partial Y}, \tag{24}$$

$$\frac{\sigma_0 c_p}{L}\frac{\partial \Sigma_{22}}{\partial T} = \frac{\lambda c_p}{a}\frac{\partial V_1}{\partial X} + \frac{(\lambda+2\mu)c_p}{w}\frac{\partial V_2}{\partial Y}, \tag{25}$$

$$\frac{\sigma_0 c_p}{L}\frac{\partial \Sigma_{12}}{\partial T} = \frac{\sigma_0 c_p}{L}\frac{\partial \Sigma_{21}}{\partial T} = \frac{\mu c_p}{w}\frac{\partial V_1}{\partial Y} + \frac{\mu c_p}{a}\frac{\partial V_2}{\partial X}. \tag{26}$$

The natural choice of the scale for stresses follows from Eqs. (22) and (23)

$$\sigma_0 = \rho c_p^2 = \lambda + 2\mu. \tag{27}$$

Such a choice of the characteristic stress σ_0 reduces the governing equations to

$$\frac{1}{L}\frac{\partial V_1}{\partial T} = \frac{1}{a}\frac{\partial \Sigma_{11}}{\partial X} + \frac{1}{w}\frac{\partial \Sigma_{12}}{\partial Y}, \tag{28}$$

$$\frac{1}{L}\frac{\partial V_2}{\partial T} = \frac{1}{a}\frac{\partial \Sigma_{21}}{\partial X} + \frac{1}{w}\frac{\partial \Sigma_{22}}{\partial Y}. \tag{29}$$

$$\frac{1}{L}\frac{\partial \Sigma_{11}}{\partial T} = \frac{1}{a}\frac{\partial V_1}{\partial X} + \frac{\lambda}{w(\lambda+2\mu)}\frac{\partial V_2}{\partial Y}, \tag{30}$$

$$\frac{1}{L}\frac{\partial \Sigma_{22}}{\partial T} = \frac{\lambda}{a(\lambda+2\mu)}\frac{\partial V_1}{\partial X} + \frac{1}{w}\frac{\partial V_2}{\partial Y}, \tag{31}$$

$$\frac{1}{L}\frac{\partial \Sigma_{12}}{\partial T} = \frac{1}{L}\frac{\partial \Sigma_{21}}{\partial T} = \frac{\mu}{w(\lambda+2\mu)}\frac{\partial V_1}{\partial Y} + \frac{\mu}{a(\lambda+2\mu)}\frac{\partial V_2}{\partial X}. \tag{32}$$

In the absence of shear stresses ($\mu = 0$), the normal stress components are identical ($\Sigma_{11} = \Sigma_{22} = \Sigma$) and the dimensionless governing equations are independent of material parameters

$$\frac{1}{L}\frac{\partial V_1}{\partial T} = \frac{1}{a}\frac{\partial \Sigma}{\partial X}, \tag{33}$$

$$\frac{1}{L}\frac{\partial V_2}{\partial T} = \frac{1}{w}\frac{\partial \Sigma}{\partial Y}. \tag{34}$$

$$\frac{1}{L}\frac{\partial \Sigma}{\partial T} = \frac{1}{a}\frac{\partial V_1}{\partial X} + \frac{1}{w}\frac{\partial V_2}{\partial Y}, \tag{35}$$

Such equations are applicable in optics and acoustics.

4. Numerical simulations

The governing equations are solved numerically by means of the conservative finite-volume wave-propagation algorithm, which was proposed by LeVeque (1997, 2002) and modified by Berezovski et al. (2000); Berezovski & Maugin (2001, 2002) for the application to the propagation of discontinuities. We consider the propagation of a plane wave in the computational domain 1000 $\times$ 220 space steps. The monochromatic plane wave is generated at the left boundary. The slit placement begins from 500 spaces steps in all cases. The boundary conditions at lateral boundaries are periodic up to the end of the slit placement. The non-reflective boundary conditions are applied at the rest of lateral boundaries as well as at the right boundary. The details of boundary conditions are presented earlier (Berezovski et al., 2015).

The results of calculations are shown for 1400 time steps in order to avoid the influence of the reflection from the left boundary (the Courant number is equal to 1 in all the simulations). This is why the results are shown starting from 400 space steps.

4.1. Optics

Classical optics is characterized by the extremely short wavelength ($L \ll a, L \ll w$). In this limiting case all unknowns become time-independent. The problem is reduced therefore to geometrical optics. Nevertheless, we can consider here a hypothetical situation with $L = a = w$, which can be relevant to THz region (Kampfrath et al., 2013, e.g.). However, we keep the walls of the slit to be rigid and impenetrable.

In this case the dimensionless equations are independent of geometrical scales (Eqs. (33)-(35)). The corresponding single-slit diffraction picture is shown in

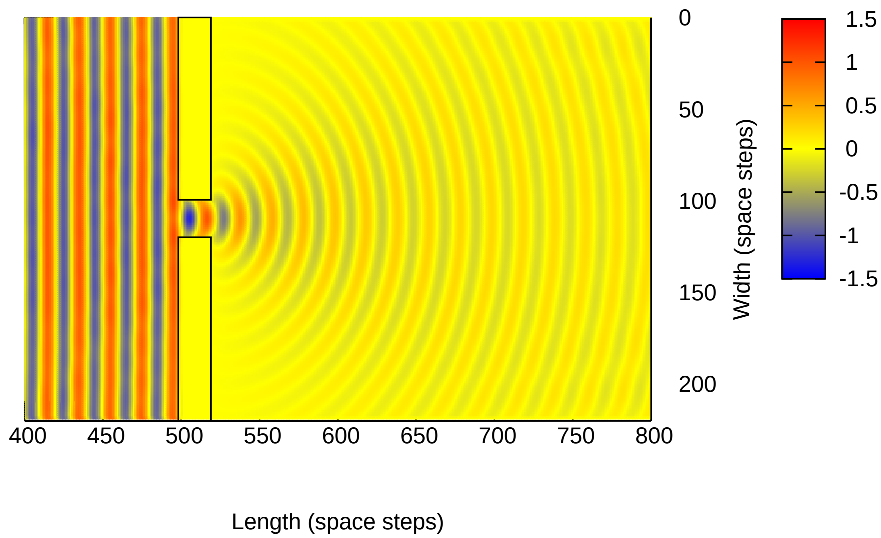

Figure 1: Single-slit diffraction. Slit width and thickness are equal to the wavelength.

Fig. 1. The boundaries of the plate forming the slit are opaque. This suggests that there is no reflection from boundaries. Such a typical illustration of the single-slit diffraction can be found elsewhere (Crowell, 2003, e.g.).

4.2. Acoustics

In acoustics, all the space scales may have the same order of magnitude. Again, in the "universal" case ($L = a = w$) the wave propagation is independent not only of material parameters, but also of geometrical scales. The dimensionless governing equations are remained the same as Eqs. (33)-(35). The plate forming the slit is assumed rigid, i.e., normal velocities are zero at boundaries of the plate. The diffraction picture for the "universal" acoustic case is represented in Fig. 2. The difference from the case of optics is the formation of a wave pattern upstream the slit due to reflection. Downstream the slit the diffraction pictures for classical optics and acoustics are similar in the "universal" case. Comparing the stress distribution along the centerline downstream the slit, we observe the difference in amplitude and small shift in phase for optical and acoustic cases (Fig. 3).

Let us consider the influence of the variation of the width of the plate forming

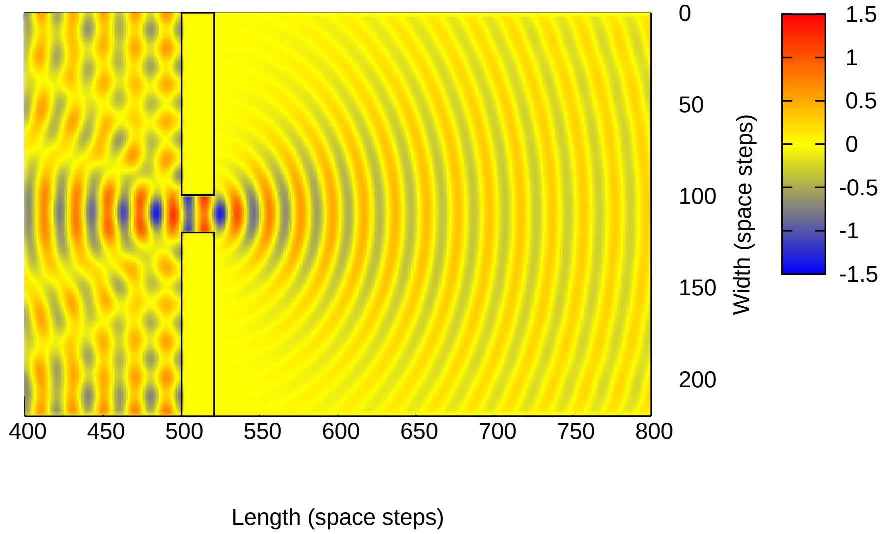

Figure 2: Single-slit diffraction in acoustics. Slit width and thickness are equal to the wavelength.

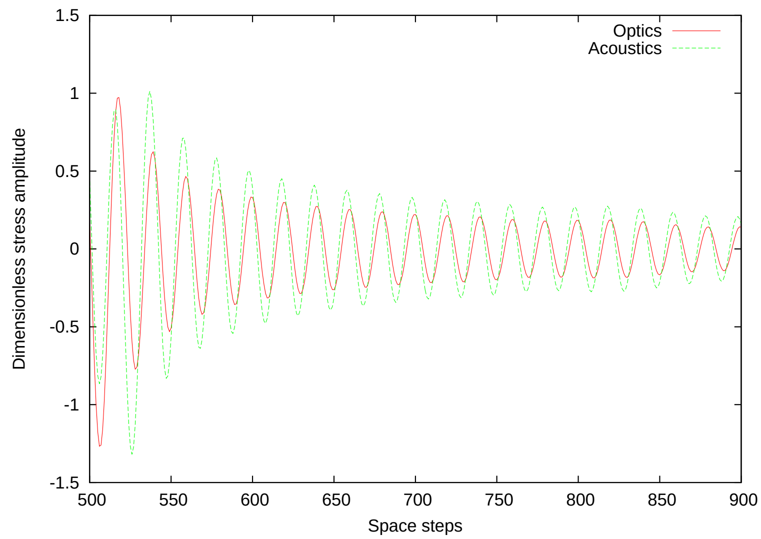

Figure 3: Centerline stress distribution for "universal" single-slit diffraction.

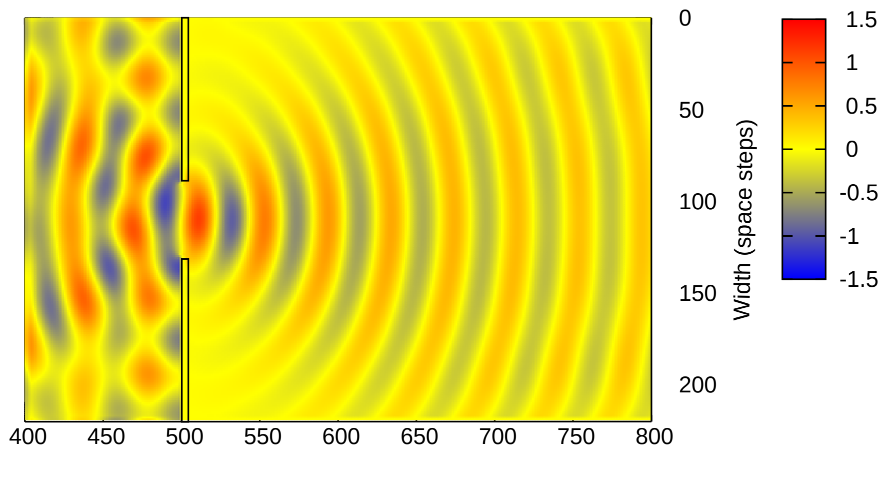

Figure 4: Single-slit diffraction in acoustics. Slit width is equal to the wavelength. Slit thickness is 10 times less.

the slit. If the width of the plate is much less than the slit size ($w \ll a$ and $w \ll L$) we arrive at large slit aperture case. The dimensionless equations become independent of the coordinate Y inside the slit, i.e. the problem is one-dimensional in space

$$\frac{1}{L}\frac{\partial V_1}{\partial T} = \frac{1}{a}\frac{\partial \Sigma}{\partial X}, \tag{36}$$

$$\frac{\partial \Sigma}{\partial Y} = 0. \tag{37}$$

$$\frac{\partial V_2}{\partial Y} = 0, \tag{38}$$

$$\frac{1}{L}\frac{\partial \Sigma}{\partial T} = \frac{1}{a}\frac{\partial V_1}{\partial X}. \tag{39}$$

The diffraction picture shown in Fig. 4 demonstrates a big difference in the longitudinal stress patterns upstream and downstream the slit.

Another limiting case corresponds to $a \ll w$. This means that the slit is relatively narrow. Accordingly, the obtained one-dimensional problem inside the slit is independent of the coordinate X:

$$\frac{\partial \Sigma}{\partial X} = 0, \tag{40}$$

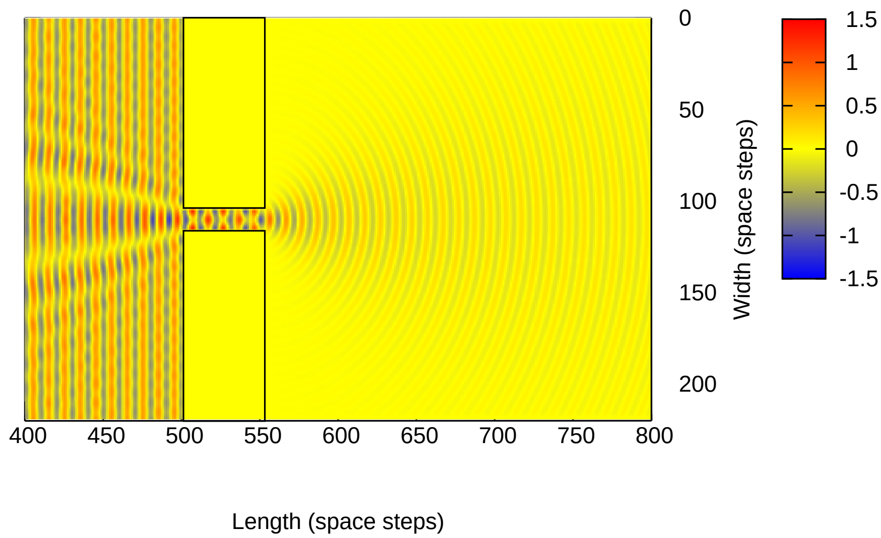

Figure 5: Single-slit diffraction in acoustics. Slit width is equal to the wavelength. Slit thickness is 5 times larger than the wavelength.

$$\frac{1}{L}\frac{\partial V_2}{\partial T} = \frac{1}{w}\frac{\partial \Sigma}{\partial Y}. \tag{41}$$

$$\frac{\partial V_1}{\partial X} = 0, \tag{42}$$

$$\frac{1}{L}\frac{\partial \Sigma}{\partial T} = \frac{1}{w}\frac{\partial V_2}{\partial Y}. \tag{43}$$

Certainly, two-dimensional equations (33)-(35) are valid upstream and downstream the slit. The corresponding diffraction image can be seen in Fig. 5. It looks much more similar to the "universal" case than to the case with large slit aperture.

In spite of the observable distinction between Figs. 2, 4 and 5, it is possible to represent the centerline stress distribution downstream the slit for all cases reinstating the wavelength and arranging the position of the slit. Such comparison shows the similarity in the reinstated stress distribution (Fig. 6). The latter means that the "universal" diffraction picture represents well all the possible cases of the acoustic single-slit diffraction. The geometrical scales can be harmonized by a corresponding transformation of results.

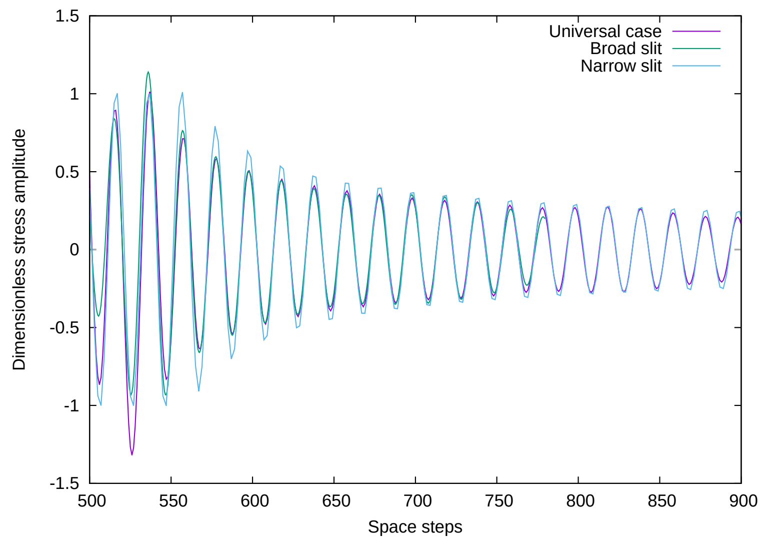

Figure 6: Centerline stress distribution for single-slit diffraction in different cases.

4.3. Elasticity

In elastic case governing Eqs. (32)-(32) are valid. Choosing the carrier material as Nickel and the material of the plate forming the slit as Lucite, we can start again with the "universal" case where all the scales are equal ($L = a = w$). The properties of Nickel are chosen as follows: ρ=8900 kg/m^3, c_p=6040 m/s, c_s=3000 m/s, and properties of Lucite are, correspondingly: ρ=1100 kg/m^3, c_p=2610 m/s, c_s=1140 m/s. The corresponding distribution of the longitudinal stress looks similarly to what we have seen in the acoustical case (Fig. 7).

The evident differences are induced by the distinct reflection and transmission conditions at elastic and rigid walls. If we turn to the large slit aperture case ($w \ll a, w \ll l$), the result still keeps the similarity with the acoustics case downstream the slit as it is observed in Fig. 8.

However, for the narrow slit the similarity between acoustic and elastic cases is much less evident (Fig. 9). This is confirmed by the comparison of the centerline distribution of the longitudinal stress for narrow, broad and "universal" slits shown in Fig. 10.

In order to check how the change in material properties of grating affects the

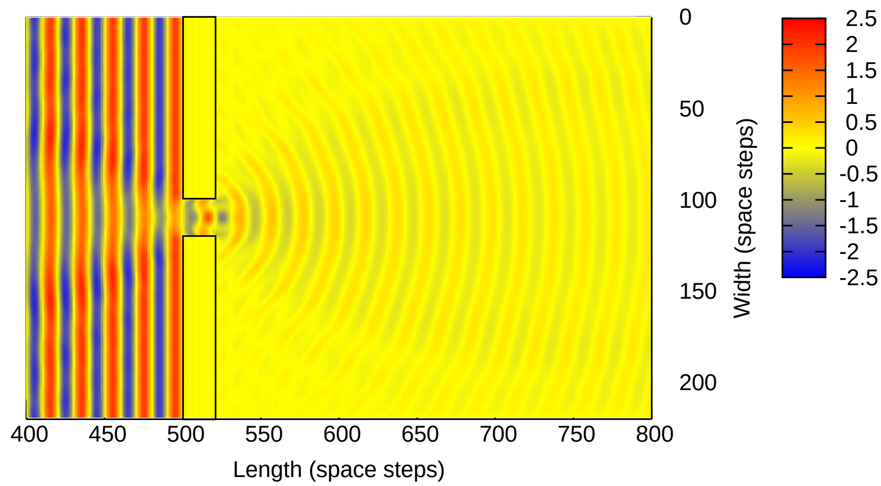

Figure 7: Single-slit diffraction in elasticity (Ni-Lu case). Slit width and thickness are equal to the wavelength.

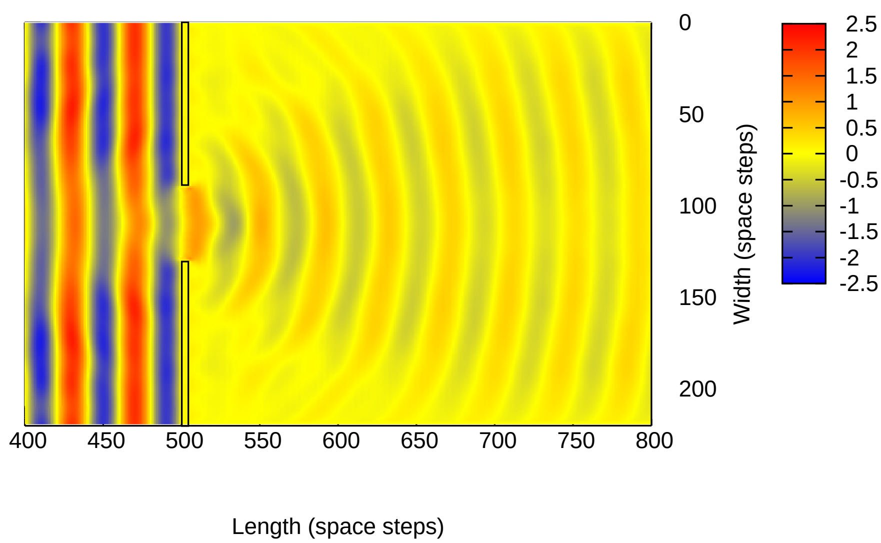

Figure 8: Single-slit diffraction in elasticity (Ni-Lu case). Slit width is equal to the wavelength. The thickness is 10 times less.

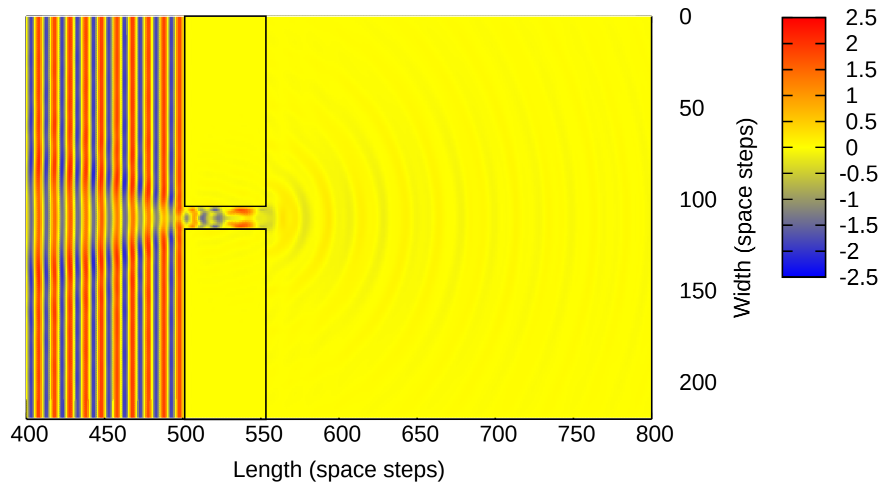

Figure 9: Single-slit diffraction in elasticity (Ni-Lu case). Slit width is equal to the wavelength. The thickness is 5 times larger than the wavelength.

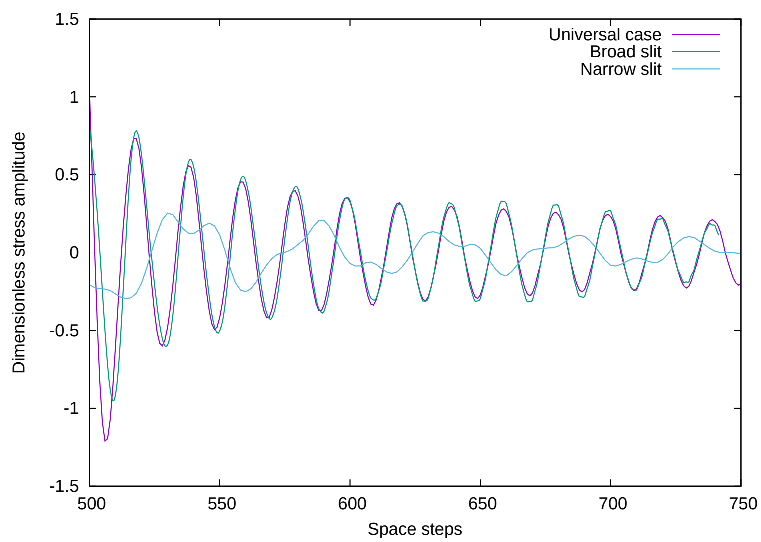

Figure 10: Centerline stress distribution for single-slit elastic diffraction in different cases.

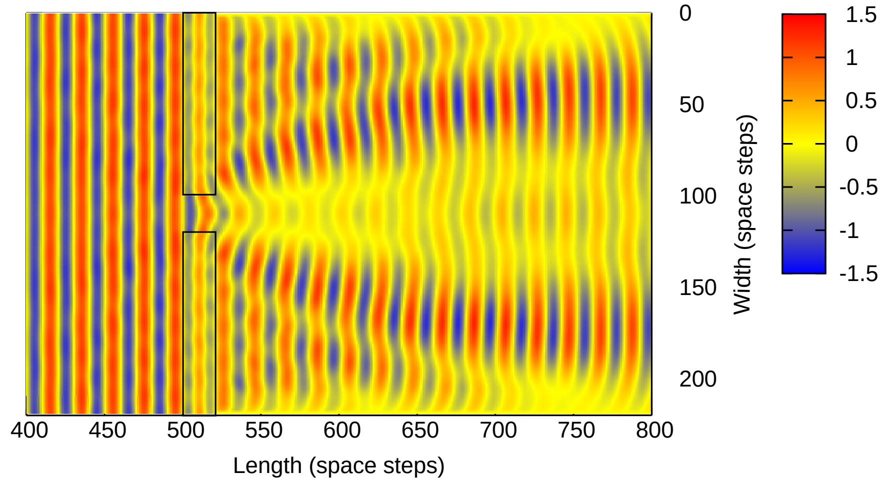

Figure 11: Single-slit diffraction in elasticity (Ni-Zn case). Slit width and thickness are equal to the wavelength.

diffraction picture, it is sufficient to consider the "universal" case with another material for the grating. For such a comparison we have chosen Zinc as the grating material. The corresponding longitudinal stress distribution is presented in the Fig. 11.

The difference between the cases Ni-Zn and Ni-Lu is evident. The stress distribution differs also along the centerline, as it can be observed in Fig. 12. If the stress distribution forms beats in the case of Ni-Zn, it is slowly decreases its magnitude in the case of Ni-Lu.

4.4. Acousto-elastic case

In the case of elastic slit in acoustic (water) medium we consider again the "universal" geometry with equal scales. In order to manifest the acousto-elastic effects clearly we choose silicone rubber as the material forming the slit.

The diffraction picture (Fig. 13) has no big difference from the standard acoustic case with rigid slit walls (Fig. 2) downstream the slit. However, the elastic slit walls start to vibrate due to the interaction with acoustic waves. The time history of the slit edge displacement shows that there appear two kinds of vibrations as it is observed in Fig. 14. Here the displacement of

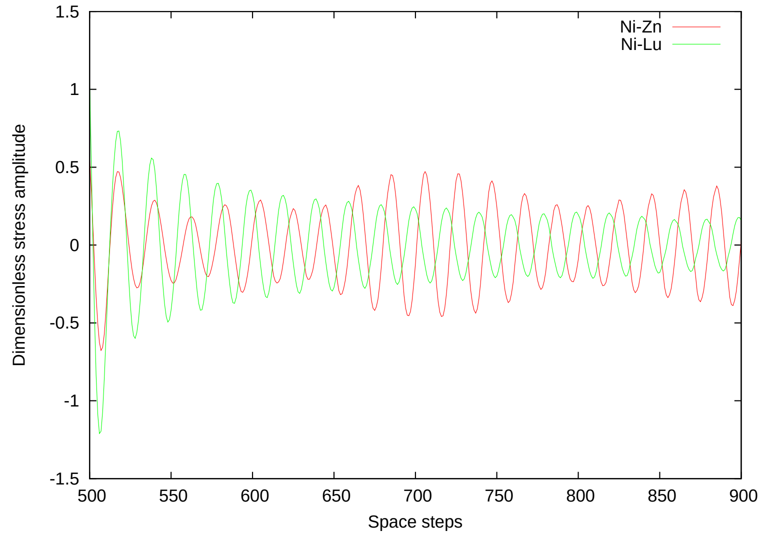

Figure 12: Centerline stress distribution for single-slit elastic diffraction for Ni-Zn and Ni-Lu.

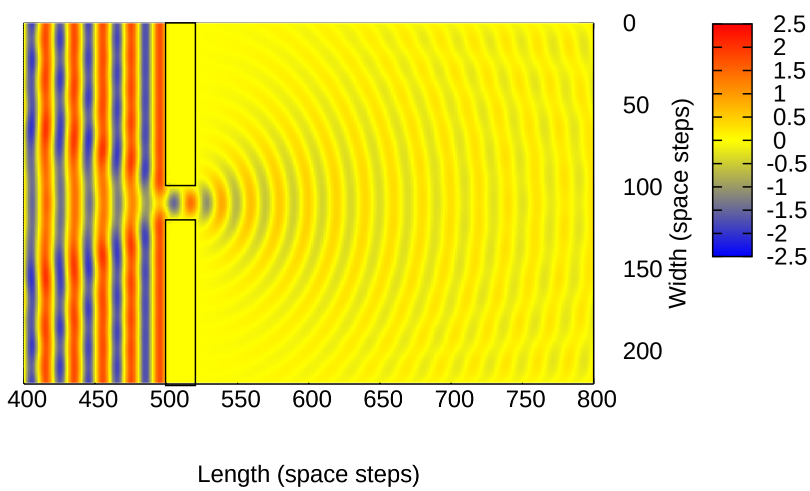

Figure 13: Single-slit diffraction in acousto-elastic case. Elastic slit width and thickness are equal to the wavelength.

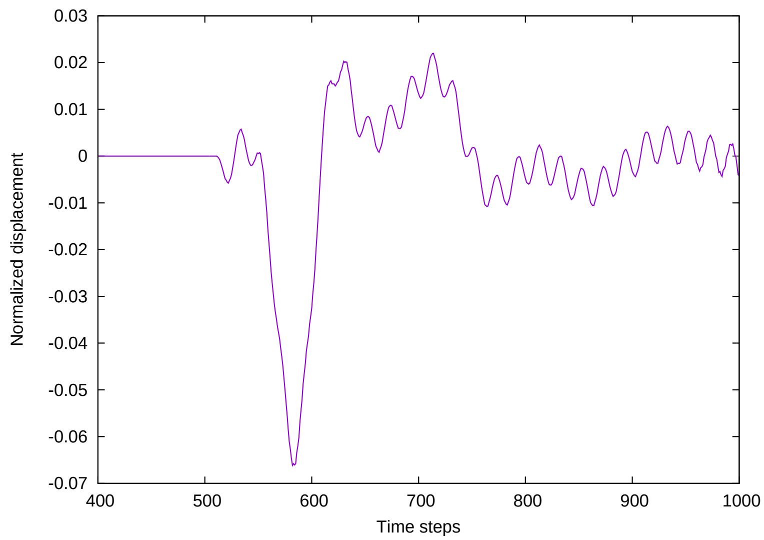

Figure 14: Time history of slit edge displacement.

the edge is normalized by the amplitude of the incident wave. As one can conclude, the global motion of the slit edges is influenced by small vibrations of a higher frequency induced by the waves in the material of the elastic slit. Similar vibrations can serve as the origin of the significant difference in the diffraction patterns for various material compositions in the completely elastic case (Figs. 7 and 11).

5. Conclusions

Growing interest to phononic crystals (Pennec et al., 2010; Deymier, 2013), acoustic metamaterials (Guenneau et al., 2007; Hussein et al., 2014), acoustic cloacking (Norris, 2008; Guenneau et al., 2011), and acoustic transmission enhancement (Christensen et al., 2010; Hao et al., 2012; Wang et al., 2014) is the reason to get a more closer look on the diffraction of waves in elastic solids. We have applied the well established finite volume wave-propagation algorithm (LeVeque, 2002; Berezovski et al., 2008) as a tool for the computation of various boundary value problems arising in the simplest diffraction case due to changes in geometry and properties of media.

In this paper we compare results of numerical calculations of plane wave propagation through a single slit in optical, acoustic, and elastic cases. Numerical simulations of the classical problem of the single slit diffraction show the similarity between optical and acoustic cases, as expected. Both cases are governed by the same equations (33)-(35), but the conditions at the boundaries of the plate forming the slit are different. This difference results in the distinct wave fields upstream of the slit. It is remarkable that results for the "universal" or "uniform" formulation of the single slit problem, where equality in the incident wavelength, the slit width, and its thickness provides the independence from geometrical scales, can represent the results for geometrically non-uniform problems after a suitable transformation.

At the same time, the single slit diffraction using elastic materials shows essentially different features. In this case the governing equations are more general ((28)-(32)) and applicable both to the matrix material and to the plate forming the slit. As a result, there is no more possibility to reduce results for non-uniform scales to the stress distribution in the geometrically uniform case. Moreover, the variation of material parameters changes the stress distribution drastically. This is an effect of elastic waves propagating inside the plate forming the slit. Such an effect is absent in classical optics and acoustics because of the assumed opaqueness or rigidity of the plate.

The observed difference between acoustic and elastic cases is unavoidable and should be taken into account in the topological optimization of composites for the controlling of elastic waves. Such a control is necessary for the redistribution of energy in a desired way in bodies under impact loading.

Acknowledgments

The research was supported by the EU through the European Regional Development Fund and by the Estonian Research Council project PUT434.

References

Achenbach, J. (1984). *Wave Propagation in Elastic Solids*. Elsevier.

Auld, B. A. (1973). *Acoustic Fields and Waves in Solids*. Wiley-Interscience.

Barber, J. R. (2009). *Elasticity*. Springer.

Benenson, W., Harris, J. W., Stöcker, H., & Lutz, H. (2002). *Handbook of Physics*. Springer Science & Business Media.

Berezovski, A., Engelbrecht, J., & Berezovski, M. (2015). Pattern formation of elastic waves and energy localization due to elastic gratings. *International Journal of Mechanical Sciences*, *101*, 137–144.

Berezovski, A., Engelbrecht, J., & Maugin, G. (2000). Thermoelastic wave propagation in inhomogeneous media. *Archive of Applied Mechanics*, *70*, 694–706.

Berezovski, A., Engelbrecht, J., & Maugin, G. A. (2008). *Numerical Simulation of Waves and Fronts in Inhomogeneous Solids*. World Scientific.

Berezovski, A., & Maugin, G. (2001). Simulation of thermoelastic wave propagation by means of a composite wave-propagation algorithm. *Journal of Computational Physics*, *168*, 249–264.

Berezovski, A., & Maugin, G. A. (2002). Thermoelastic wave and front propagation. *Journal of Thermal Stresses*, *25*, 719–743.

Berezovski, A., Tang, W.-X., & Wan, W. (2014). Elastic wave Talbot effect in solids with inclusions. *Mechanics Research Communications*, *60*, 21–26.

Christensen, J., Martín-Moreno, L., & García-Vidal, F. J. (2010). Enhanced acoustical transmission and beaming effect through a single aperture. *Physical Review B*, *81*, 174104.

Crowell, B. (2003). *Newtonian Physics* volume 1. Light and Matter.

De Hoop, A. T. (2008). *Handbook of Radiation and Scattering of Waves: Acoustic Waves in Fluids, Elastic Waves in Solids, Electromagnetic Waves: with Corrections*. Academic Press.

Deymier, P. A. (2013). *Acoustic Metamaterials and Phononic Crystals*. Springer Science & Business Media.

Graff, K. F. (1975). *Wave Motion in Elastic Solids*. Courier Dover Publications.

Guenneau, S., McPhedran, R. C., Enoch, S., Movchan, A. B., Farhat, M., & Nicorovici, N.-A. P. (2011). The colours of cloaks. *Journal of Optics*, *13*, 024014.

Guenneau, S., Movchan, A., Pétursson, G., & Ramakrishna, S. A. (2007). Acoustic metamaterials for sound focusing and confinement. *New Journal of Physics*, *9*, 399.

Hao, R., Qiu, C., Ye, Y., Li, C., Jia, H., Ke, M., & Liu, Z. (2012). Transmission enhancement of acoustic waves through a thin hard plate embedded with elastic inclusions. *Applied Physics Letters*, *101*, 021910.

Harris, J. G. (2010). *Elastic Waves at High Frequencies: Techniques for Radiation and Diffraction of Elastic and Surface Waves*. Cambridge University Press.

Hellier, C., & Hellier, C. (2001). *Handbook of Nondestructive Evaluation* volume 10. McGraw-Hill New York.

Hussein, M. I., Leamy, M. J., & Ruzzene, M. (2014). Dynamics of phononic materials and structures: historical origins, recent progress, and future outlook. *Applied Mechanics Reviews*, *66*, 040802.

Kampfrath, T., Tanaka, K., & Nelson, K. A. (2013). Resonant and nonresonant control over matter and light by intense terahertz transients. *Nature Photonics*, *7*, 680–690.

LeVeque, R. J. (1997). Wave propagation algorithms for multidimensional hyperbolic systems. *Journal of Computational Physics*, *131*, 327–353.

LeVeque, R. J. (2002). *Finite Volume Methods for Hyperbolic Problems*. Cambridge University Press.

Martin, P. A. (2006). *Multiple Scattering: Interaction of Time-harmonic Waves with N Obstacles*. Cambridge University Press.

Mow, C.-C., & Pao, Y.-H. (1971). *The diffraction of elastic waves and dynamic stress concentrations*. Technical Report R-482-PR Rand Corporation Santa Monica, CA.

Norris, A. N. (2008). Acoustic cloaking theory. *Proceedings of the Royal Society A: Mathematical, Physical and Engineering Science*, *464*, 2411–2434.

Pennec, Y., Vasseur, J. O., Djafari-Rouhani, B., Dobrzyński, L., & Deymier, P. A. (2010). Two-dimensional phononic crystals: Examples and applications. *Surface Science Reports*, *65*, 229–291.

Rayleigh, L. (1887). On the maintenance of vibrations by forces of double frequency, and on the propagation of waves through a medium endowed with a periodic structure. *The London, Edinburgh, and Dublin Philosophical Magazine and Journal of Science*, *24*, 145–159.

Talbot, H. F. (1836). Facts relating to optical science. no. IV. *The London and Edinburgh Philosophical Magazine and Journal of Science*, *9*, 401–407.

Wang, J., Yuan, B., Cheng, Y., & Liu, X. (2014). Unidirectional acoustic transmission in asymmetric bulls eye structure. *Science China Physics, Mechanics & Astronomy*, *58*, 1–5.

Young, T. (1804). The Bakerian lecture: Experiments and calculations relative to physical optics. *Philosophical Transactions of the Royal Society of London*, *94*, 1–16.